



The quasi-biennial oscillation in a warmer climate: sensitivity to different gravity wave parameterizations

Sebastian Schirber · Elisa Manzini ·
Thomas Krismer · Marco Giorgetta

Received: 6 June 2014 / Accepted: 25 August 2014 / Published online: 5 September 2014
© The Author(s) 2014. This article is published with open access at Springerlink.com

Abstract In order to simulate the quasi-biennial oscillation (QBO) with a realistic period and amplitude, general circulation models commonly include parameterizations of small scale gravity waves (GW). In this work, we explore how different GW parameterization setups determine the response of QBO properties to a warmer climate. Atmosphere-only experiments in both present day and warmer climate serve as testbed to analyze the effect of four different GW parameterization setups, active in the tropics. Having tuned the GW parameterizations to produce a realistic QBO in present day climate, we analyze changes of QBO properties in the warmer climate. The QBO period decreases in two parameterization setups by ~30 %, while the QBO period remains unchanged in the remaining two parameterization setups. In all parameterization setups, the QBO amplitude in the warmer climate weakens below 10 hPa but shows different behaviour above 10 hPa. We show that changes in QBO amplitude and changes in QBO period are inconsistent among experiments. In the chosen experimental design, the inconsistent future change in QBO properties among the suite of experiments depends solely on the choice of the GW parameterization setup.

Keywords Quasi-biennial oscillation · Gravity waves · Parameterization · Climate change

1 Introduction

The quasi-biennial oscillation (QBO) of equatorial zonal winds is a prominent feature of stratospheric dynamics. The QBO is driven downward—against the general tropical upwelling—by waves which emanate from the troposphere and travel upwards into the stratosphere. At the alternating shear zones of the QBO, the waves break, deposit momentum and cause a downward propagation of the wind maxima. The waves driving the QBO range from large scale Kelvin and Rossby-gravity waves to smaller scale gravity waves (GW) with shorter horizontal wavelength. Dunkerton (1997) show that the contribution of intermediate inertia-GWs and mesoscale GWs is necessary to produce a QBO with realistic period and amplitude. For a more detailed description on the forcing and the physical mechanisms of the QBO (see the review paper by Baldwin et al. 2001).

Apart from being a phenomena to study wave—mean flow interactions in a fluid on a rotating sphere, the QBO influences other parts of the atmosphere, in both the stratosphere and the troposphere. Holton and Tan (1980) show that the easterly phase of the QBO is associated with weakening of the northern wintertime stratospheric polar vortex. In the troposphere, the QBO influences tropical cyclone tracks (Ho et al. 2009), the boreal summer monsoon (Giorgetta et al. 1999) and tropical deep convection (Collimore et al. 2003; Liess and Geller 2012). Recent work shows that the QBO reveals predictability in the tropics (Pohlmann et al. 2013) and weak predictability in the north Atlantic sector (Scaife et al. 2014). Potential changes of the QBO in a warmer climate will therefore influence tropospheric processes.

S. Schirber (✉) · E. Manzini · T. Krismer · M. Giorgetta
Max Planck Institute for Meteorology,
Bundesstr. 53, 20146 Hamburg, Germany
e-mail: sebastian.schirber@mpimet.mpg.de

E. Manzini
e-mail: elisa.manzini@mpimet.mpg.de

T. Krismer
e-mail: thomas.krismer@mpimet.mpg.de

M. Giorgetta
e-mail: marco.giorgetta@mpimet.mpg.de

Depending on the horizontal resolution, general circulation models (GCM) resolve only a fraction of the waves necessary to produce a QBO. Several GCMs, with sufficiently high horizontal resolution, succeed in generating a QBO or produce QBO-like oscillations (Hamilton et al. 1999; Watanabe 2005; Watanabe and Miura 2008). Since a high model resolution demands high computational costs, many GCMs exhibit a coarser resolution than necessary to cover the full range of waves driving the QBO. Due to the limited resolution of current GCMs, the effect of unresolved GWs generally needs to be parameterized before GCMs can produce a QBO (Scaife et al. 2000; Giorgetta et al. 2002; Shibata and Deushi 2005; Richter 2014). GW parameterizations remain an essential ingredient in many GCMs which generate a QBO, especially in the case of fully coupled state-of-the-art earth system models which are usually employed to run comprehensive climate change simulations.

The QBO behaviour in a future, warmer climate is dependent on the employed model. On one hand, Giorgetta and Doege (2005) show a shortening of the QBO period in a doubled CO₂ climate, while prescribing an increased activity of parameterized GWs in the warmer climate. On the other hand, two variants of the Model for Interdisciplinary Research on Climate (MIROC) show a lengthening of the QBO period, along with a decrease in the QBO amplitude under future climate conditions (Kawatani et al. 2011; Watanabe and Kawatani 2012). Analyzing four models (HadGEM2-CC, MPI-ESM-MR and two variants of MIROC-ESM) of the Coupled Model Intercomparison Project Phase 5 (CMIP5), Kawatani and Hamilton (2013) associate an increased upwelling with a decrease in QBO amplitude in the lower stratosphere. While the decrease in QBO amplitude is consistent within all four models and also with observations, changes in QBO period differ between models, even in sign. While HadGEM2-CC shows a shorter QBO period, the two MIROC-ESM variants show a longer QBO period in a future climate, and MPI-ESM-MR shows a lengthening before the year 2000 followed by a shortening of the QBO period thereafter (Kawatani and Hamilton 2013, supplementary information).

All four models, analyzed by Kawatani and Hamilton (2013), employ GW parameterizations with prescribed, constant GW sources which are generally tuned, within the range of observational constraints, in present day climate. In this work, we analyze the sensitivity of QBO changes, due to a warmer climate, to different tropical GW parameterization setups within the same model framework. In the presence of a GW parameterization, the QBO simulated in a GCM is driven by three forcing mechanisms: (1) resolved, large scale waves, (2) unresolved, parameterized GW and (3) advection which is

dominated by vertical upwelling. Since we aim to isolate the effect of different GW parameterizations on the QBO, we use identical boundary conditions across the suite of parameterization setups. In detail, we not only prescribe identical atmospheric boundary conditions like sea surface temperature (SST), but we also use the identical GW parameterization in the extratropics. This experimental setup aims at minimizing the changes of the remaining two forcing agents of the QBO, the resolved waves and the upwelling, within the suite of different GW parameterization setups. We are therefore able to associate changes in QBO properties with the choice of the GW parameterization setup.

This is the first time that multiple GW parameterizations in the tropics are systematically analyzed within the same model framework with respect to QBO changes in a warmer climate. This approach helps to quantify the contribution of GW parameterizations to the spread in simulated QBO period changes of CMIP5 models.

2 Experimental setup

We use the atmospheric general circulation model ECHAM6 (Stevens et al. 2013), the latest version of the atmospheric component of the earth system model developed at the Max Planck Institute for Meteorology (MPI-ESM) (Giorgetta et al. 2013). The simulations performed here use a spectral truncation at wave number 63 and an associated Gaussian grid of $\sim 1.9^\circ$ resolution. The vertical grid with a spacing of roughly 700 m in the lower stratosphere resolves the atmosphere up to 0.01 hPa. For more details on the middle atmospheric circulation of ECHAM6 (see Schmidt et al. 2013) with a description of the QBO and the resolved waves in Krismer et al. (2013). For comparison of QBO properties in Sect. 3.1 we use the reanalysis product ERA-Interim (Dee et al. 2011).

We perform atmosphere-only simulations for two different climates, a present day climate and a warmer climate. The boundary conditions for the present day climate correspond to AMIP conditions, defined as in Taylor et al. (2012), including observed sea surface temperatures (SST) and sea ice concentrations for the period 1979 until 2008. The warmer climate uses the same SST patterns as in AMIP, but uniformly increased by 4 K (AMIP4K), while all other boundary conditions remain unchanged. We omit additional changes in CO₂ concentrations in our experimental setup because changes in SSTs dominate QBO changes in a warmer climate (Kawatani et al. 2012). Unless otherwise stated we analyze monthly, zonal and meridional, $\pm 10^\circ$ latitude, mean data of a 30 year period for each of the experiments.

2.1 Setup of GW parameterizations

In this study we compare four different setups of non-orographic GW parameterizations in the tropics. In the extratropics all four parameterization setups share the identical GW parameterizations. The different GW parameterization setups consist of either a GW propagation scheme with fixed GW sources or a combination of a GW propagation scheme coupled to an interactive GW source parameterization. The GW parameterization setups or parts of the GW parameterization setups are employed in various GCMs of different modeling centers. (1|Hines) is the standard parameterization setup of ECHAM6 and the model version employed for CMIP5. We set up (2|AD) as an analogue to (1|Hines), such that (2|AD) also launches a prescribed, constant spectrum of GWs at the same height as (1|Hines). However the propagation scheme’s design and wave breaking criteria differ among the two GW parameterization setups. (3|AD+Beres) is a GW parameterization setup recently implemented into ECHAM6 (Schirber et al. 2014) with the aim to gain physical coupling between the modeled convection and the excited GWs. Finally we design (4|ADfixBeres) to analyze the effect of the interactive source spectrum of (3|AD+Beres). We summarize the different GW parameterization setups in Table 1 and explain the detailed parameterization setups individually in the following paragraphs.

1|Hines The standard ECHAM6 model version, which is part of CMIP5, employs the GW scheme after Hines which is based on the Doppler spread theory (Hines 1997a, b). The schemes launches a broad band spectrum of waves at 600 hPa with constant amplitude in time and longitude. In

Table 1 Overview of different GW parameterization setups: the experiment acronym as used in this work, the propagation scheme, the intermittency value ϵ of the propagation scheme AD99, the horizontal wavelength λ_h , the nature of momentum flux sources (interactive or prescribed), the waves’ launch level, details on the symmetry of the source spectrum and the phase speed c_{max} where the momentum flux source spectrum peaks

Acronym	Hines	AD	AD+Beres	ADfixBeres
Propagation	Hines	AD	AD	AD
ϵ	–	0.001	0.0025	0.0025
λ_h	126 km	100 km	100 km	100 km
Sources	Prescribed	Prescribed	Interactive	Prescribed
Launch level	600 hPa	600 hPa	Cloud top	130 hPa
Spectrum shape	Symmetric	Symmetric	Asymmetric	As AD+Beres
c_{max}	–	8 m/s	$\pm\sim 20$ m/s	As AD+Beres

Note that “as AD+Beres” refers to the zonal, meridional and time mean

the CMIP5 model setup, a latitudinal amplitude enhancement is introduced around the equator in order to obtain a QBO with a realistic period (Schmidt et al. 2013). The latitudinal enhancement is achieved by setting u_{rms} , the parameter for the GW source strength, to 1.2 m/s near the equator, latitude $|\Phi| \leq 5^\circ$, while $u_{rms} = 1$ m/s outside the tropics.

For the following three parameterization setups, we disable the Hines scheme in the tropics ($\pm 20^\circ$ latitude) and keep it active only in the extratropics. Since the following three GW parameterization setups excite waves only in the tropics, all four parameterizations share the identical Hines GW parameterization setup in the extratropics.

2|AD The spectral GW propagation scheme after Alexander and Dunkerton 1999, hereafter AD99) is based on the assumption that momentum fluxes carried by waves are deposited entirely at the initial onset of linear instability, which corresponds to the breaking criterion after Lindzen (1981). We use the scheme with modifications reducing the scheme’s computational cost (Ortland and Alexander 2006). The GW source spectrum of momentum flux B remains constant in space and time and is calculated by equation (29) of AD99

$$B(c) = B_m \rho \left(\frac{c}{c_{max}} \right) \exp \left(1 - \left| \frac{c}{c_{max}} \right| \right) \tag{1}$$

with phase speed c , peak phase speed $c_{max} = 8$ m/s, density ρ and maximum flux magnitude $B_m = 7 \times 10^{-4} \text{ m}^2/\text{s}^2$. The shape of the chosen source spectrum lies within the range of observed spectra (Alexander and Holton 1997; Piani and Durran 2001; Alexander et al. 2006; Kuester et al. 2008).

3|AD+Beres We couple the convection based GW source parameterization after Beres et al. (2004) to the GW propagation routine AD99. On each model grid point and each timestep, the GW source parameterization generates an interactive source spectrum based on the latent heating properties and the background wind. The scheme’s advantages over a prescribed, constant spectrum are twofold. First, the shape of source spectrum is generated interactively dependent on physical properties and therefore, secondly, the source spectrum includes spatial and temporal variability. Waves are launched at the top of the convective heating, ranging from 3.5 up to 17 km. For details on the implementation of the scheme in ECHAM6 and the scheme’s physical coupling to the sources (see Schirber et al. 2014).

4|ADfixBeres We extract the zonal, meridional and time mean spectrum of the AD+Beres AMIP experiment and prescribe this spectrum as a fixed and constant

spectrum for AD99. In present day climate AD+Beres and ADfixBeres show an identical source spectrum. While the source spectrum for ADfixBeres remains constant in both present and warmer climate, the source spectrum of AD+Beres will change in a warmer climate, due to its interactive nature. Therefore the setup ADfixBeres allows to analyze the effect of the interactive source spectrum of AD+Beres in the warmer climate. The ADfixBeres setup launches waves at 130 hPa which corresponds to the height where the Beres scheme shows the peak momentum fluxes in ECHAM6 (Schirber et al. 2014). We consider the high temporal and spatial intermittency of the Beres source parameterization in present climate by launching waves only on a small spatial fraction of gridpoints in ADfixBeres. Note that the tuning of the propagation scheme AD99 in ADfixBeres is identical to AD+Beres, with horizontal wavelength $\lambda_h = 100$ km and intermittency factor $\epsilon = 0.0025$.

We tune all four parameterization setups individually to simulate the QBO of present day climate, with a focus on the QBO period. While the parameterizations provide a variety of tuning parameters, we restrict our tuning to two aspects in the three AD based parameterization setups. First, the intermittency ϵ and the horizontal wavelength λ_h of AD99 influence the breaking levels where GWs become convectively unstable. Second, the amplitude of the source spectrum determines the amount of emitted source momentum flux. Relevant parameters for the latter aspect are B_m for AD and c_f and L for Beres with details in Schirber et al. (2014).

2.2 Source spectra of momentum flux

The momentum flux source spectra of the three AD based parameterization setups are shown in Fig. 1. The spectra B are scaled by density ρ and calculated at the respective launch levels, ranging from 600 hPa in AD to 130 hPa ADfixBeres and distributed over the entire troposphere in AD+Beres. Since the AD experiment launches waves at a much lower level than AD+Beres and ADfixBeres, the amount of source momentum flux in AD is an order of magnitude larger than AD+Beres and ADfixBeres (see Fig. 1). However in the lower stratosphere below the QBO relevant heights (see Fig. 8), the absolute amount of momentum flux for each of the four parameterization setups lies within the range of observations, with mean absolute momentum fluxes varying between 1 and 5 mPa (Sato and Dunkerton 1997; Piani et al. 2000; Grimsdell et al. 2010; Geller et al. 2013).

The symmetric source spectrum of AD peaks at 8 m/s, while the interactively generated spectrum of AD+Beres is asymmetric and shows a peak around 20 m/s phase speed. Due to its physically based character, the source spectrum

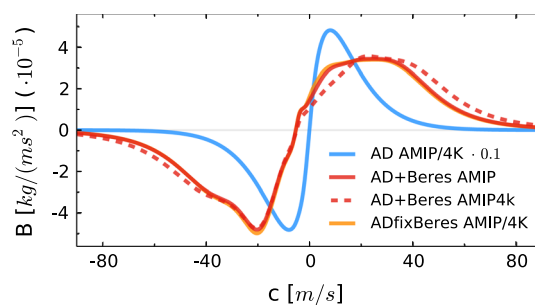


Fig. 1 Momentum flux (B) source spectrum as a function of horizontal phase speed (c) for the experiments AD, AD+Beres and ADfixBeres; time, zonal and meridional mean. While the spectra of AD (blue) and ADfixBeres (orange) remain unchanged under AMIP and AMIP4K boundary conditions, the interactive source spectrum of AD+Beres (solid red) changes under the warmer climate of AMIP4K (dashed red). Note that the spectrum of AD is scaled by 0.1 for visualization reasons. ADfixBeres is hidden for the most part by AD+Beres AMIP

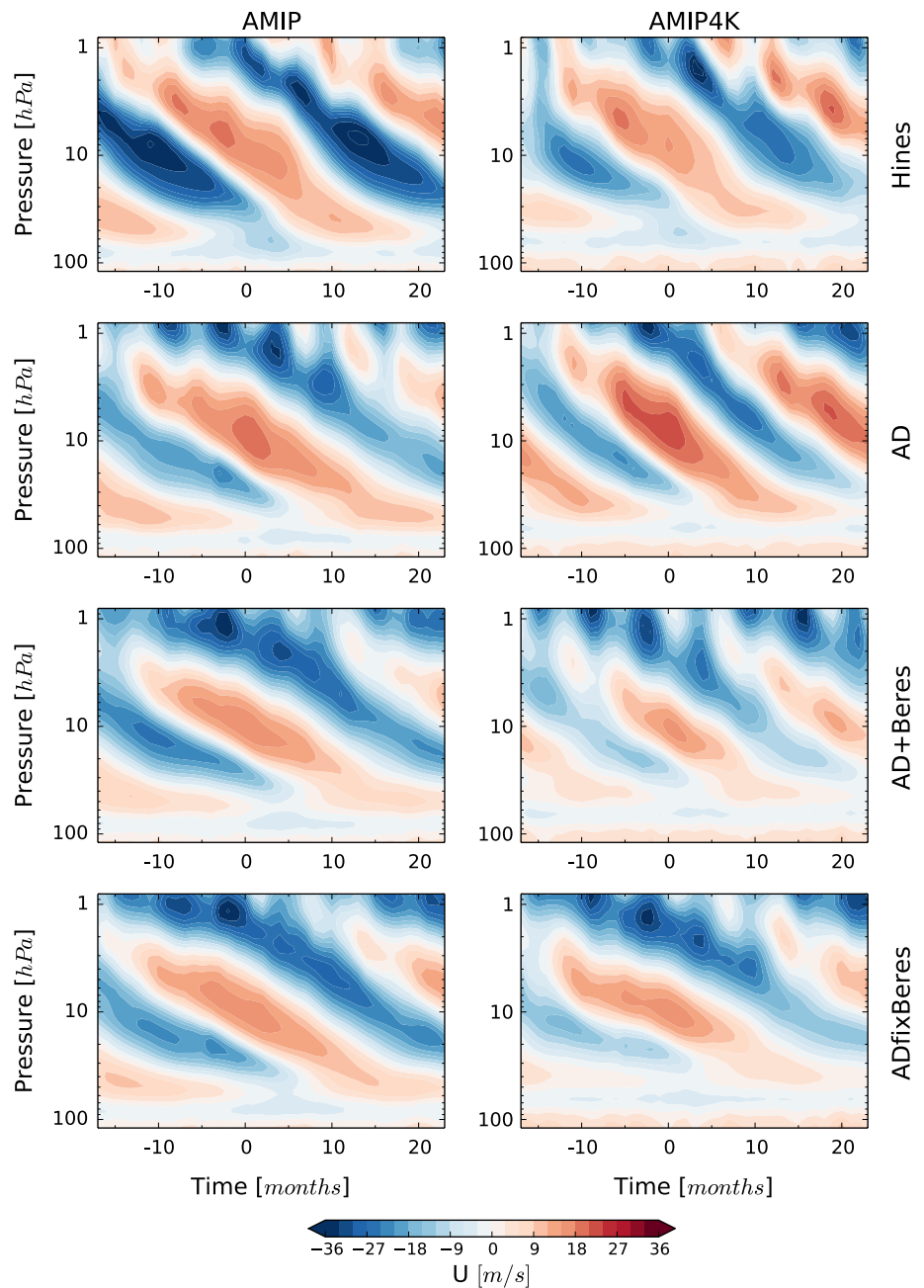
of AD+Beres in AMIP4K is different to the source spectrum under AMIP boundary conditions, while both the AD and ADfixBeres source spectra are by construction constant under different boundary conditions. Note that the source spectrum of Hines does not appear in Fig. 1, because the parameterization's design does not allow a straightforward calculation of a momentum flux source spectrum as a function of horizontal phase speed. As for AD and ADfixBeres, we set the source characteristics of Hines constant under the different boundary conditions of AMIP and AMIP4K.

3 Results

3.1 QBO characteristics in a warmer climate

In the warmer climate several QBO characteristics are changing in the different parameterization setups. The QBO composites in Fig. 2 show differences in QBO amplitude, in the vertical extent of easterly and westerly jets, in their downward propagation speeds, in the QBO period and in the position of the tropopause. In order to systematically analyze the QBO changes across the suite of parameterization setups, we focus on the two main QBO characteristics: The QBO period and the QBO amplitude. We determine the QBO period calculating the onsets of the westerly jet at 20 hPa in time. Changing the vertical level or analyzing the onset of the easterly jet gives qualitatively similar results for the QBO period. We determine the QBO amplitude calculating the maximum value of the easterly and the westerly jet of each QBO oscillation on each level. Given a timeseries of 30 years, we then average over the maximum jet values and also calculate a standard deviation on each level for both the easterly and the westerly jet.

Fig. 2 QBO composites for the experiments Hines, AD, AD+Beres and ADfixBeres, each for present day (*left column*) and warmer climate (*right column*). The onset of the westerly jet at 20 hPa is chosen as the criterion to calculate the composite, compiled from zonal and meridional mean zonal wind



In the present climate the mean QBO periods among the different parameterization setups range between ~26 and ~29 months which lies in the observed range of QBO periods with a mean of ~28 months, indicated by ERA-Interim (see Fig. 3). In the warmer climate the QBO period remains, to a first approximation, constant for the parameterization setups Hines and ADfixBeres. However, the QBO period becomes shorter by roughly 30 % or 8–9 months for the AD and AD+Beres parameterization setup. While the spread of the distribution increases in both Hines and ADfixBeres in a warmer climate, the spread of

the distribution in AD and AD+Beres remains unchanged under AMIP and AMIP4K boundary conditions.

While we present the QBO period changes, we further highlight the individual descent durations of the easterly and the westerly jet (see Fig. 4). The descent durations of the easterly and the westerly QBO jet remain roughly constant for Hines and ADfixBeres, while the QBO jet descent durations decrease for AD and AD+Beres. In the latter two cases, note that both easterly and westerly descent durations change comparably. Therefore we show that not one particular phase of the QBO contributes to the reduction in

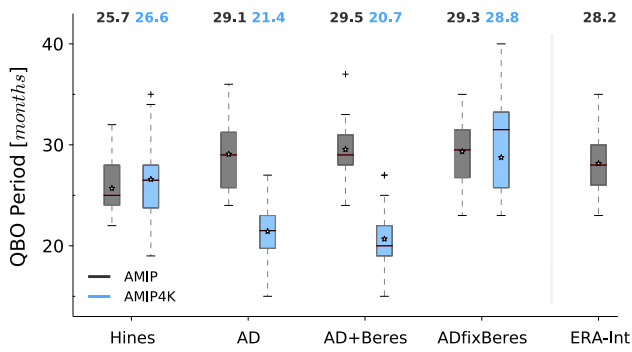


Fig. 3 Distribution of QBO periods for the experiments Hines, AD, AD+Beres and ADfixBeres, each for present day (black) and warmer climate (blue), and the reanalysis ERA-Interim for present day climate. Periods are determined at the onset of the westerly jet at 20 hPa, compiled from zonal and meridional mean zonal wind. The distribution median is depicted by the horizontal line within each box, the distribution mean by the star whose value is drawn above. The box covers the interquartile range, distribution outliers are denoted by plus symbol

QBO period, but a decreased descent duration in both easterly and westerly QBO jets.

The changes in QBO amplitude in the warmer climate depend on the parameterization setup, but also show one common feature. In all parameterization setups, the easterly jet below 10 hPa becomes weaker in the warmer climate (see Fig. 5). While the easterly jet loses strength also above 10 hPa in AD+Beres, an amplitude reduction above 10 hPa is less clear for Hines, AD and ADfixBeres. The westerly jet below 20 hPa remains unchanged for Hines and AD, whereas the westerly jet becomes weaker by ~40 % for AD+Beres and ADfixBeres below 20 hPa. Above 20 hPa the westerly jet increases for Hines and AD while it remains rather unchanged for AD+Beres and ADfixBeres. We don't observe any consistent, detailed

trend in variance of QBO amplitude among the different parameterization setups. However generally speaking, we qualitatively state that the variance of QBO amplitude tends to increase rather than decrease in a warmer climate. Note that a longer simulation with more resolved QBO cycles would be needed for a more precise statement on the variance of QBO amplitude.

3.2 Resolved waves and upwelling

The changes in resolved waves, due to a warmer climate, exhibit a consistent behaviour among the simulations of all parameterization setups. In the regions below the QBO, we show the vertical component F_z of the Eliassen–Palm (EP) flux vector as a measure of the resolved wave activity (see Fig. 6). In the warmer climate, F_z increases for both westerly and easterly waves while the westerly waves show a stronger increase in magnitude than the easterly waves (see left panel in Fig. 6). Since the QBO is driven by a range of waves with different scales, we show the integral of F_z for the two components. A more detailed spectral analysis, which we do not present here, shows that the increase in resolved wave activity occurs at all wave numbers and is not dominated by a particular wave mode. The combined magnitude of easterly and westerly resolved waves, the absolute value $|F_z|$, increases in the warmer climate (see center panel of Fig. 6). We quantify the spread of the changes in $|F_z|$ among the simulations of the different parameterization setups in the right panel of Fig. 6. The standard deviation $\sigma_{\Delta|F_z|}$ of $\Delta|F_z|$ among the different parameterization setups is an order of magnitude smaller than $\Delta|F_z|$. Therefore, the differences of $\Delta|F_z|$ between the parameterization setups are small, with ~10 %, compared to changes between present day and the warmer climate in $|F_z|$.

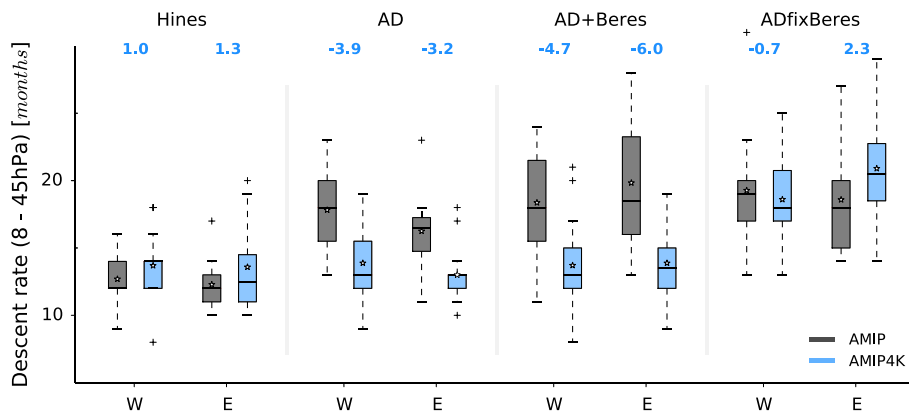


Fig. 4 Distribution of QBO jet descent rates for the experiments Hines, AD, AD+Beres and ADfixBeres, each for present day (black) and warmer climate (blue), compiled from zonal and meridional mean zonal wind. The descent rate is determined for the westerly

(W) and easterly (E) jet by calculating the time the wind maxima take from 8 hPa until 45 hPa. The difference (AMIP4K-AMIP) in the mean is drawn above. For details on box properties (see Fig. 3)

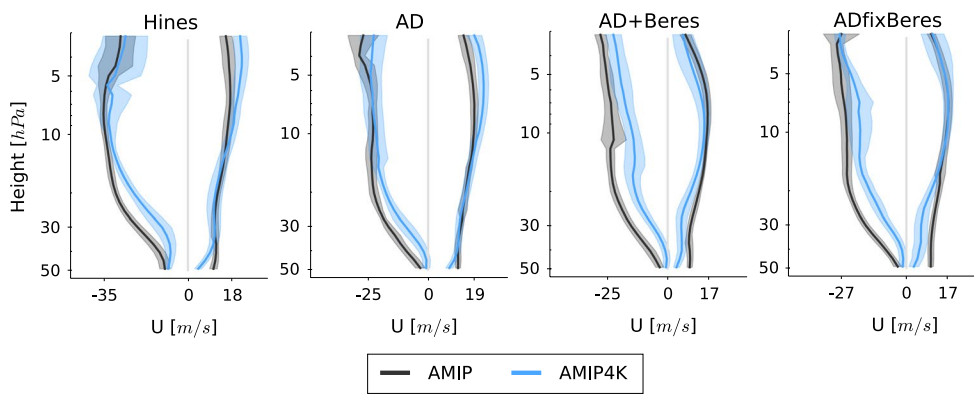


Fig. 5 Vertical QBO amplitude profiles for the experiments Hines, AD, AD+Beres and ADfixBeres, each for present day (black) and warmer climate (blue), compiled from zonal and meridional mean wind. The amplitude is calculated as the mean maximum wind

speed of the QBO easterly ($U < 0$) and westerly ($U > 0$) jets on each vertical level. The shading illustrates the range of two standard deviations σ . The labels on the x-axis show the maximum value of the AMIP profiles

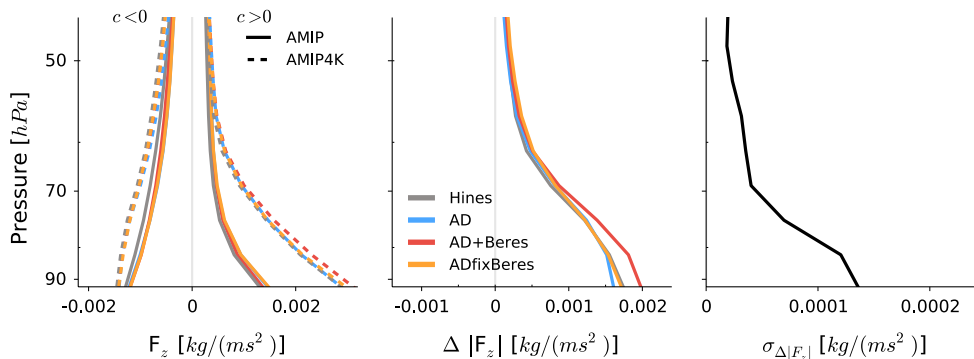


Fig. 6 Vertical profile of vertical component F_z of the spectral EP-Flux vector for the experiments Hines, AD, AD+Beres and ADfixBeres; time (10 years, based on 6 hourly data), zonal and meridional mean. F_z shows the integral over frequencies and wave numbers. Left panel F_z of easterly ($c < 0$) and westerly ($c > 0$) waves for pre-

sent day (solid) and warmer climate (dashed). Center panel change of the absolute value $\Delta|F_z| = |F_z|_{AMIP4K} - |F_z|_{AMIP}$ from present day climate to the warmer climate, with $|F_z| = |F_{z,c < 0}| + |F_{z,c > 0}|$. Right panel standard deviation σ of $\Delta|F_z|$ of the four parameterization setups

The change in upwelling Δw^* , due to a warmer climate, also exhibits a consistent behaviour among all parameterization setups. The profiles of the residual vertical velocity w^* of a transformed Eulerian mean analysis shows a minimum at ~ 50 hPa, increasing above and below (see left panel in Fig. 7). In the warmer climate, the profiles exhibit a general shift to higher values of w^* , while the increase in the lower stratosphere exceeds the increase at higher stratospheric levels (see center panel in Fig. 7). The standard deviation $\sigma_{\Delta w^*}$ of Δw^* among the different parameterization setups is an order of magnitude smaller than Δw^* (see right panel in Fig. 7).

Summarizing the above results, we see that the response of the resolved waves and the upwelling to a changing climate is independent of the applied GW parameterization setup. The changes among the simulations of the different GW parameterization setup are more than an order of

magnitude smaller than the changes from present day climate to the warmer climate. This result, which we desire by the design of the experimental setup, allows to relate changes in the QBO to the different GW parameterization setups.

3.3 GW momentum fluxes and acceleration due to GWs

To complete the picture of QBO-driving mechanisms, we show the contribution of the different GW parameterization setups. The GW momentum flux (B) profiles reflect the differences between properties of the individual parameterization setups (see left panel in Fig. 8). AD and Hines launch GWs at 600 hPa in the middle troposphere, ADfixBeres launches waves at 130 hPa and AD+Beres launches GWs interactively at the top of the modeled convection. Therefore AD, Hines and ADfixBeres show a monotonic decrease in

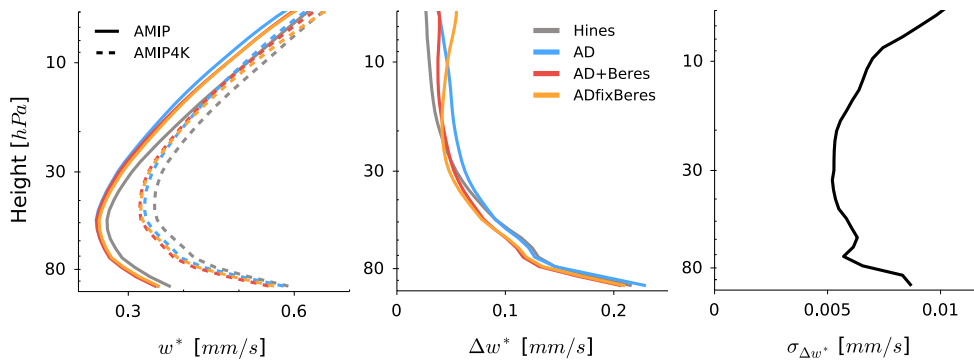


Fig. 7 Vertical profile of residual vertical velocity w^* of a transformed Eulerian mean analysis for the experiments Hines, AD, AD+Beres and ADfixBeres; time, zonal and meridional ($\pm 25^\circ$ latitude) mean data. *Left panel* w^* for present day (solid) and warmer

climate (dashed). *Center panel* increase of w^* from present day climate to warmer climate, with $\Delta w^* = w^*_{AMIP4K} - w^*_{AMIP}$. *Right panel* standard deviation σ of Δw^* of the four parameterization setups

GW momentum fluxes with height, whereas the momentum fluxes in Beres peak in the high troposphere where deep convective clouds inject large values of momentum fluxes. For a detailed distribution of momentum flux launch levels of the Beres scheme in ECHAM6 (see Schirber et al. 2014).

In a warmer climate momentum fluxes B in Hines and ADfixBeres remain, as a first approximation, unchanged. This is illustrated by the small difference of solid and dashed profiles of Hines and ADfixBeres in the left panel of Fig. 8. The absolute changes $\Delta|B|$ between the warmer and the present day climate show neither a systematic increase nor a systematic decrease, but follow the zero-change line in the right panel in Fig. 8. However the parameterization setup AD shows less momentum fluxes below and within the lower QBO domain in AMIP4K. Given that the GW sources in AD are constant in present day and warmer climate, a reduction in momentum fluxes in the lower stratosphere indicates stronger tropospheric wave filtering for AD in a warmer climate. The peak in the GW momentum flux profile of AD+Beres

shifts to higher vertical levels, following the increased vertical extent of deep convection in a warmer climate. This vertical shift of launch levels in AD+Beres leads to a relative decrease in momentum fluxes below 100 hPa and a relative increase in momentum fluxes above 100 hPa (see right panel in Fig. 8). The peak values of B in AD+Beres, however, remain essentially unchanged in the warmer climate.

After the momentum flux profiles of the different GW parameterization setups, we present the resulting tendency of zonal wind due to GWs ($\frac{\partial U}{\partial t}|_{GW}$). Please note, that an analysis of the wind tendency is only of limited informative value in this comparison of different GW parameterization setups. Even though it is the tendency, and not the momentum fluxes, that ultimately accelerates the QBO jets and drives the QBO, the tendency depends at the same time on the detailed wind profile of the modeled QBO. In both present and warmer climate, the QBOs and therefore the wind profiles that the GW parameterization react to, differ among the four parameterization setups. Therefore, the tendency profiles will necessarily differ among the GW parameterization setups. As a consequence we don't compare the tendency profiles of the different GW parameterization setups with each other, but we focus on the relative change between present and warmer climate for each GW parameterization setup individually.

We calculate the absolute amount of GW tendency $|\frac{\partial U}{\partial t}|_{GW}$ as the sum of the tendency of westerly GWs $|\frac{\partial U}{\partial t}|_{GW,c>0}$ and the tendency of easterly GWs $|\frac{\partial U}{\partial t}|_{GW,c<0}$. The amount of GW tendency $|\frac{\partial U}{\partial t}|_{GW}$, scaled by density, peaks in the lower domain of the QBO at ~ 80 – 100 hPa and decreases above (see left panel on Fig. 9). The relative change of GW tendency due to the warmer climate

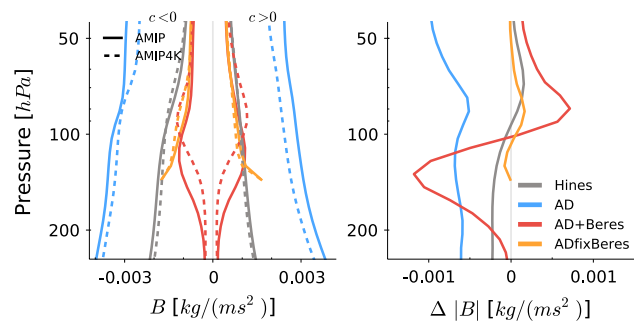


Fig. 8 Vertical profile of gravity wave momentum flux (B) for the experiments Hines, AD, AD+Beres and ADfixBeres; time, zonal and meridional mean data. *Left panel* B of easterly ($c < 0$) and westerly ($c > 0$) for present day (solid) and warmer climate (dashed). *Right panel* change of total momentum flux $\Delta|B| = |B|_{AMIP4K} - |B|_{AMIP}$, with $|B| = |B_{c<0}| + |B_{c>0}|$

$$\Delta \left| \frac{\partial U}{\partial t} \right|_{GW} = \frac{\left| \frac{\partial U}{\partial t} \right|_{GW,AMIP4K} - \left| \frac{\partial U}{\partial t} \right|_{GW,AMIP}}{\left| \frac{\partial U}{\partial t} \right|_{GW,AMIP}}$$

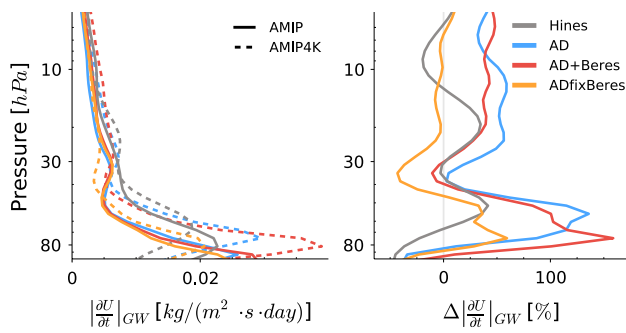


Fig. 9 Vertical profile of zonal wind tendency due to GWs ($\frac{\partial U}{\partial t}|_{GW}$) for the experiments Hines, AD, AD+Beres and ADfixBeres; time, zonal and meridional mean data; $\frac{\partial U}{\partial t}$ is scaled by density ρ . Left panel absolute GW tendency with $|\frac{\partial U}{\partial t}|_{GW} = |\frac{\partial U}{\partial t}|_{GW,c>0} + |\frac{\partial U}{\partial t}|_{GW,c<0}$ for present day (solid) and warmer climate (dashed). Right panel relative change of absolute GW tendency $\Delta|\frac{\partial U}{\partial t}|_{GW}$

is shown in the right panel of Fig. 9. In the warmer climate, the parameterization setups ADfixBeres and Hines show both an increase and decrease of $|\frac{\partial U}{\partial t}|_{GW}$, depending on the vertical level. However AD and AD+Beres show a systematic increase in GW tendency in the warmer climate, with an increase of ~50 % above 25 hPa and exceeding 100 % in the lower QBO domain between 40 and 80 hPa.

4 Summary and discussion

In this work we address the sensitivity of QBO changes, due to a warmer climate, to four different GW parameterization setups which are summarized in Table 1. We run atmosphere-only experiments with prescribed SSTs in both present day (AMIP) and a 4 K warmer climate (AMIP4K). The only difference in the model setups are the different GW parameterizations in the tropics, while the GW parameterization in the extratropics remains identical. This experimental setups minimizes the spread of future changes of the two model-intrinsic QBO driving mechanisms, the resolved waves and the upwelling, among the four parameterization setups (see Figs. 6, 7). Therefore, the differences in QBO changes in a warmer climate are driven by the differences in GW parameterizations. While all parameterization setups are tuned to simulate a QBO with properties of present day climate, we analyze changes of the QBO in a warmer climate.

While both Hines and ADfixBeres show small changes in QBO period in the warmer climate, both AD and AD+Beres show a reduction in QBO period by 8–9 months (see Fig. 3). In the two cases of a QBO period shortening, we observe an increase in exerted acceleration in QBO regions (see right panel in Fig. 8). Due to a weaker easterly jet, the QBO amplitude below 10 hPa shows a reduction in

all four parameterization setups (see Fig. 5), which is consistent with results from Kawatani and Hamilton (2013). Analyzing the overall changes in QBO amplitude among the different parameterization setups, we see that Hines and AD on one hand, and AD+Beres and ADfixBeres on the other hand show a rather similar behaviour in QBO amplitude in the warmer climate.

Summarizing changes in both QBO properties, we show that changes in QBO period are not related to changes in QBO amplitude. For example, both AD and AD+Beres exhibit a reduction in QBO period, while their changes in QBO amplitude differs, except for the easterly jet below 10 hPa. Given the amplitude reduction of the easterly jet descends faster in the warmer climate compared to the present day climate, because a weaker jet requires less forcing to descend. However we show in Fig. 4, that the descent duration of both the easterly and westerly jets reduce comparably in AD and AD+Beres. This result underscores the previous statement, that changes in QBO amplitude are independent of changes in QBO period.

Our results show that the response of the QBO to a warmer climate is sensitive not only to the choice of the GW parameterization setups, like Hines versus AD, but also to the tuning and to individual properties of the GW parameterizations. Both AD and ADfixBeres use the propagation scheme after Alexander and Dunkerton, both with a fixed source spectrum. The two parameterizations setups however differ in the launch level, the spectral shape and the tuning of the propagation. The difference in properties of the GW parameterization suffices to lead to no change in QBO period for ADfixBeres and a reduction in QBO period for AD. However, properties of the source spectrum or the tuning of the propagation scheme alone do not determine future QBO changes either. Both AD+Beres and ADfixBeres employ a very similar source spectrum in the future climate and identical tuning of the propagation scheme (see Fig. 1). Yet, the QBO period only changes for AD+Beres in the future climate.

We finalize this section with a more detailed discussion on the different response of AD+Beres and ADfixBeres to the warmer climate. The experimental setup AD+Beres is the only setup which considers changes in the GW sources due to a warmer climate, while ADfixBeres uses the diagnosed AD+Beres source spectrum of present day climate in both the present and warmer climate. The substantial differences in QBO period changes between these two experimental setups highlights the impact of a physically based and therefore changing GW source parameterization. We discuss possible reasons for the differences between AD+Beres and ADfixBeres. The source spectrum in AD+Beres increases slightly in the warmer climate (see Fig. 1), but the overall amount of excited momentum flux

at the source level does not increase substantially, indicated by the similar peak values for AD+Beres for present and warmer climate in the left panel of Fig. 8. However, due to a deeper vertical extent of convection in the warmer climate, the launching height of the peak source momentum flux in AD+Beres increases by roughly 20 hPa, see the left panel of Fig. 8. A higher launch level entails less wave filtering and more available momentum flux that drives the QBO. We do not identify a clear reason for the difference between AD+Beres and ADfixBeres, but we speculate that the changes in launch level in AD+Beres partly cause the changes between the two experimental setups.

5 Conclusion

On one hand, both the experimental setups Hines and ADfixBeres show no change in QBO period in a warmer climate and both Hines and ADfixBeres show no change in exerted acceleration on the QBO. Therefore we conclude that, in these two cases, the increased forcing of resolved waves is balanced by the increased upwelling, which counteracts wave forcing.

On the other hand, both AD and AD+Beres show a decrease in QBO period in a warmer climate. In the case of AD+Beres, the total amount of emanating momentum flux does not increase substantially (see Fig. 1) and left panel in Fig. 8, but the mean launching height of GWs increases in the warmer climate. In the case of AD, the amount of momentum flux below the QBO domain decreases in the warmer climate. The decrease in GW momentum flux opposes the assumed increase in GW tendency, as expected from a shorter QBO period in the warmer climate. In the warmer climate, however, both AD and AD+Beres do exert more acceleration in QBO regions than in present day climate (see right panel in Fig. 9). Since the QBO period decreases for AD and AD+Beres, we conclude that the increase in resolved wave forcing and the increase in exerted acceleration due to GWs outweighs the increase in upwelling.

We are not able to explain why certain GW parameterization setups change specific QBO properties. However we can state the differences in the experimental setup of GW parameterizations that lead to changes in QBO properties. Results of this work suggest that changes in QBO properties in a warmer climate do not only depend on the GW scheme, but also on differences in source spectrum properties like the launch level, the spectral shape, the physical link to the sources, and the tuning of the propagation scheme. Small changes in any of the mentioned properties can lead to pronounced changes in QBO properties in a warmer climate. In a warmer climate, QBO properties and in particular the QBO period are highly sensitive to the employed GW parameterization, its detailed setup and its tuning.

Outlook and suggestions Given the strong sensitivity of future QBO changes to the choice of GW parameterizations, we present three suggestions for future work on this topic.

1. Work with idealized sensitivity studies in 1D models allows to disentangle the complex feedbacks acting between the QBO-driving mechanisms and eventually help to better understand fundamental QBO mechanisms.
2. Better observations of GWs in the lower stratosphere would better constrain the tuning and properties of GW parameterizations.
3. The use of high resolution models which cover a sufficient amount of resolved waves helps to reduce the necessity of GW parameterizations. Until those high resolution models become the standard of state-of-the-art GCMs, a physical based GW parameterization like AD+Beres remains the most realistic approach.

Acknowledgments We thank the Max Planck Society and the International Max Planck Research School for Earth System Modeling. We thank Claudia Timmreck and two anonymous reviewers for providing valuable feedback on this manuscript. Simulations were carried out on the supercomputing facilities of the German Climate Computation Center (DKRZ) in Hamburg.

Open Access This article is distributed under the terms of the Creative Commons Attribution License which permits any use, distribution, and reproduction in any medium, provided the original author(s) and the source are credited.

References

- Alexander M, Holton J (1997) A model study of zonal forcing in the equatorial stratosphere by convectively induced gravity waves. *J Atmos Sci* 54:408–419
- Alexander MJ, Dunkerton TJ (1999) A spectral parameterization of mean-flow forcing due to breaking gravity waves. *J Atmos Sci* 56(24):4167–4182. doi:10.1175/1520-0469(1999)056<4167:ASPOMF>2.0.CO;2
- Alexander MJ, Richter JH, Sutherland BR (2006) Generation and trapping of gravity waves from convection with comparison to parameterization. *J Atmos Sci* 63(11):2963–2977. doi:10.1175/JAS3792.1
- Baldwin M, Gray L, Dunkerton TJ, Hamilton K, Haynes PH, Randel WJ, Holton JR, Alexander MJ, Hirota I, Horinouchi T, Jones DBA, Kinnerson JS, Marquardt C, Sato K, Takahashi M (2001) The quasi-biennial oscillation. *Rev Geophys* 39(2):179–229
- Beres JH, Alexander MJ, Holton JR (2004) A method of specifying the gravity wave spectrum above convection based on latent heating properties and background wind. *J Atmos Sci* 61(3):324–337. doi:10.1175/1520-0469(2004)061<0324:AMOSTG>2.0.CO;2
- Collimore C, Martin D, Hitchman M, Huesmann A, Waliser D (2003) On the relationship between the QBO and tropical deep convection. *J Clim* 16(15):2552–2568
- Dee DP, Uppala SM, Simmons AJ, Berrisford P, Poli P, Kobayashi S, Andrae U, Balmaseda MA, Balsamo G, Bauer P, Bechtold P, Beljaars ACM, van de Berg L, Bidlot J, Bormann N, Delsol C,

- Dragani R, Fuentes M, Geer AJ, Haimberger L, Healy SB, Hersbach H, Hólm EV, Isaksen L, Kållberg P, Köhler M, Matricardi M, McNally AP, Monge-Sanz BM, Morcrette JJ, Park BK, Peubey C, de Rosnay P, Tavalato C, Thépaut JN, Vitart F (2011) The ERA-interim reanalysis: configuration and performance of the data assimilation system. *Q J R Meteorol Soc* 137(656):553–597. doi:[10.1002/qj.828](https://doi.org/10.1002/qj.828)
- Dunkerton TJ (1997) The role of gravity waves in the quasi-biennial oscillation. *J Geophys Res* 102(D22):26,053–26,076
- Geller MA, Alexander MJ, Love PT, Bacmeister J, Ern M, Hertzog A, Manzini E, Preusse P, Sato K, Zhou T (2013) A comparison between gravity wave momentum fluxes in observations and climate models. *J Clim* 26(17):6383–6405. doi:[10.1175/JCLI-D-12-00545.1](https://doi.org/10.1175/JCLI-D-12-00545.1)
- Giorgetta MA, Doege MC (2005) Sensitivity of the quasi-biennial oscillation to CO₂ doubling. *Geophys Res Lett* 32(L08):701. doi:[10.1029/2004GL021971](https://doi.org/10.1029/2004GL021971)
- Giorgetta MA, Bengtsson L, Arpe K (1999) An investigation of QBO signals in the east Asian and Indian monsoon in GCM experiments. *Clim Dyn* 15(6):435–450. doi:[10.1007/s003820050292](https://doi.org/10.1007/s003820050292)
- Giorgetta MA, Manzini E, Roeckner E (2002) Forcing of the quasi-biennial oscillation from a broad spectrum of atmospheric waves. *Geophys Res Lett* 29(8):8–11. doi:[10.1029/2002GL014756](https://doi.org/10.1029/2002GL014756)
- Giorgetta MA, Jungclaus J, Reick CH, Legutke S, Bader J, Böttinger M, Brovkin V, Crueger T, Esch M, Fieg K, Glushak K, Gayler V, Haak H, Hollweg HD, Ilyina T, Kinne S, Kornbluh L, Matei D, Mauritsen T, Mikolajewicz U, Mueller W, Notz D, Pithan F, Raddatz T, Rast S, Redler R, Roeckner E, Schmidt H, Schnur R, Segschneider J, Six KD, Stockhause M, Timmreck C, Wegner J, Widmann H, Wieners KH, Claussen M, Marotzke J, Stevens B (2013) Climate and carbon cycle changes from 1850 to 2100 in MPI-ESM simulations for the coupled model intercomparison project phase 5. *J Adv Model Earth Syst*. doi:[10.1002/jame.20038](https://doi.org/10.1002/jame.20038)
- Grimsdell AW, Alexander MJ, May PT, Hoffmann L (2010) Model study of waves generated by convection with direct validation via satellite. *J Atmos Sci* 67(5):1617–1631. doi:[10.1175/2009JAS3197.1](https://doi.org/10.1175/2009JAS3197.1)
- Hamilton K, Wilson RJ, Hemler RS (1999) Atmosphere simulated with high vertical and horizontal resolution versions of a GCM: Improvements in the cold pole bias and generation of a QBO-like oscillation in. *J Atmos Sci* 56(22):3829–3846. doi:[10.1175/1520-0469\(1999\)056<3829:MASWHV>2.0.CO;2](https://doi.org/10.1175/1520-0469(1999)056<3829:MASWHV>2.0.CO;2)
- Hines C (1997a) Doppler-spread parameterization of gravity-wave momentum deposition in the middle atmosphere. Part 1: basic formulation. *J Atmos Sol Terr Phys* 59(4):371–386
- Hines C (1997b) Doppler-spread parameterization of gravity-wave momentum deposition in the middle atmosphere. Part 2: broad and quasi monochromatic spectra, and implementation. *J Atmos Sol Terr Phys* 59(4):387–400
- Ho CH, Kim HS, Jeong JH, Son SW (2009) Influence of stratospheric quasi-biennial oscillation on tropical cyclone tracks in the western North Pacific. *Geophys Res Lett* 36(6):1–4. doi:[10.1029/2009GL037163](https://doi.org/10.1029/2009GL037163)
- Holton J, Tan H (1980) The influence of the equatorial quasi-biennial oscillation on the global circulation at 50 mb. *J Atmos Sci* 37:2200–2208
- Kawatani Y, Hamilton K (2013) Weakened stratospheric quasi-biennial oscillation driven by increased tropical mean upwelling. *Nature* 497(7450):478–481. doi:[10.1038/nature12140](https://doi.org/10.1038/nature12140)
- Kawatani Y, Hamilton K, Watanabe S (2011) The quasi-biennial oscillation in a double CO₂ climate. *J Atmos Sci* 68(2):265–283. doi:[10.1175/2010JAS3623.1](https://doi.org/10.1175/2010JAS3623.1)
- Kawatani Y, Hamilton K, Noda A (2012) The effects of changes in sea surface temperature and CO₂ concentration on the quasi-biennial oscillation. *J Atmos Sci* 69(5):1734–1749. doi:[10.1175/JAS-D-11-0265.1](https://doi.org/10.1175/JAS-D-11-0265.1)
- Krismer TR, Giorgetta Ma, Esch M (2013) Seasonal aspects of the quasi-biennial oscillation in MPI-ESM and ERA-40. *J Adv Model Earth Syst* 5:406–421. doi:[10.1002/jame.20024](https://doi.org/10.1002/jame.20024)
- Kuester MA, Alexander MJ, Ray EA (2008) A model study of gravity waves over Hurricane Humberto (2001). *J Atmos Sci* 65(10):3231–3246. doi:[10.1175/2008JAS2372.1](https://doi.org/10.1175/2008JAS2372.1)
- Liess S, Geller MA (2012) On the relationship between QBO and distribution of tropical deep convection. *J Geophys Res* 117(D3):1–12. doi:[10.1029/2011JD016317](https://doi.org/10.1029/2011JD016317)
- Lindzen R (1981) Turbulence and stress owing to gravity wave and tidal breakdown. *J Geophys Res* 86:9707–9714
- Ortland DA, Alexander MJ (2006) Gravity wave influence on the global structure of the diurnal tide in the mesosphere and lower thermosphere. *J Geophys Res* 111(A10S10):1–15. doi:[10.1029/2005JA011467](https://doi.org/10.1029/2005JA011467)
- Piani C, Durran D (2001) A numerical study of stratospheric gravity waves triggered by squall lines observed during the TOGA COARE and COPT-81 experiments. *J Atmos Sci* 58(1997):3702–3723
- Piani C, Durran D, Alexander MJ, Holton JR (2000) A numerical study of three-dimensional gravity waves triggered by deep tropical convection and their role in the dynamics of the QBO. *J Atmos Sci* 57(22):3689–3702. doi:[10.1175/1520-0469\(2000\)057<3689:ANSOTD>2.0.CO;2](https://doi.org/10.1175/1520-0469(2000)057<3689:ANSOTD>2.0.CO;2)
- Pohlmann H, Wa Müller, Kulkarni K, Kameswarrao M, Matei D, Vamborg FSE, Kadow C, Illing S, Marotzke J (2013) Improved forecast skill in the tropics in the new MiKlip decadal climate predictions. *Geophys Res Lett* 40(21):5798–5802. doi:[10.1002/2013GL058051](https://doi.org/10.1002/2013GL058051)
- Richter J (2014) On the simulation of the quasi-biennial oscillation in the Community Atmosphere Model, version 5. *J Geophys Res Atmos* 119:3045–3062. doi:[10.1002/2013JD021122](https://doi.org/10.1002/2013JD021122)
- Sato K, Dunkerton T (1997) Estimates of momentum flux associated with equatorial Kelvin and gravity waves. *J Geophys Res* 102(D22):26,247–26,261
- Scaife A, Butchart N, Warner CD, Stainforth D, Norton W, Austin J (2000) Realistic quasi biennial oscillations in a simulation of the global climate. *Geophys Res Lett* 27(21):3481–3484
- Scaife A, Athanassiadou M, Andrews M, Arribas A, Baldwin M, Dunstone N, Knight J, MacLachlan C, Manzini E, Mueller W, Pohlmann H, Smith D, Stockdale T, Williams A (2014) Predictability of the quasi-biennial oscillation and its northern winter teleconnection on seasonal to decadal timescales. *Geophys Res Lett* 41:1–7. doi:[10.1002/2013GL059160](https://doi.org/10.1002/2013GL059160). Received
- Schirber S, Manzini E, Alexander MJ (2014) A convection based gravity wave parameterization in a general circulation model: implementation and improvements on the QBO. *J Adv Model Earth Syst* 6:264–279. doi:[10.1002/2013MS000286](https://doi.org/10.1002/2013MS000286)
- Schmidt H, Rast S, Bunzel F, Esch M, Giorgetta M, Kinne S, Krismer T, Stenchikov G, Timmreck C, Tomassini L, Walz M (2013) Response of the middle atmosphere to anthropogenic and natural forcings in the CMIP5 simulations with the Max Planck Institute Earth system model. *J Adv Model Earth Syst* 5(1):98–116. doi:[10.1002/jame.20014](https://doi.org/10.1002/jame.20014)
- Shibata K, Deushi M (2005) Partitioning between resolved wave forcing and unresolved gravity wave forcing to the quasi-biennial oscillation as revealed with a coupled chemistry–climate model. *Geophys Res Lett* 32(12):L12,820. doi:[10.1029/2005GL022885](https://doi.org/10.1029/2005GL022885)
- Stevens B, Giorgetta M, Esch M, Mauritsen T, Crueger T, Rast S, Salzmann M, Schmidt H, Bader J, Block K, Brokopf R, Fast I, Kinne S, Kornbluh L, Lohmann U, Pincus R, Reichler T, Roeckner E (2013) Atmospheric component of the mPim earth system model: ECHAM6. *J Adv Model Earth Syst* 5:1–27. doi:[10.1002/jame.20015](https://doi.org/10.1002/jame.20015)

- Taylor KE, Stouffer RJ, Meehl GA (2012) An overview of CMIP5 and the experiment design. *Bull Am Meteorol Soc* 93(4):485–498. doi:[10.1175/BAMS-D-11-00094.1](https://doi.org/10.1175/BAMS-D-11-00094.1)
- Watanabe S (2005) Kelvin waves and ozone Kelvin waves in the quasi-biennial oscillation and semiannual oscillation: A simulation by a high-resolution chemistry-coupled general circulation model. *J Geophys Res* 110(D18):D18303. doi:[10.1029/2004JD005424](https://doi.org/10.1029/2004JD005424)
- Watanabe S, Kawatani Y (2012) Sensitivity of the QBO to mean tropical upwelling under a changing climate simulated with an earth system model. *J Meteorol Soc Jpn* 90A:351–360. doi:[10.2151/jmsj.2012-A20](https://doi.org/10.2151/jmsj.2012-A20)
- Watanabe S, Miura H (2008) Development of an atmospheric general circulation model for integrated earth system modeling on the earth simulator. *J Earth Simul* 9:27–35